

FOSSILIZED BIOMATS AS THE POSSIBLE SOURCE OF HIGH NATURAL RADIONUCLIDE CONTENT AT THE JURASSIC ÚRKÚT MANGANESE ORE DEPOSIT, HUNGARY

Ildikó GYOLLAI¹, Márta POLGÁRI^{1,2*}, Lóránt BÍRÓ¹, Tamás VIGH³, Tibor KOVÁCS⁴ & Elemér PÁL-MOLNÁR⁵

¹Research Centre for Astronomy and Geosciences, Geobiomineralization and Astrobiological Research Group, Institute for Geological and Geochemical Research, Hungarian Academy of Sciences, 1112 Budapest, Budaörsi str. 45, Hungary, e-mail: rodokrozit@gmail.com, gyildi@gmail.com

²Eszterházy Károly University, Department of Natural Geography and Geoinformatics, 3300 Eger, Leányka str. 6/C, Hungary

³Mangán Ltd, Úrkút, Külterület 1. 8409 Hungary, e-mail: drvightamas@gmail.com

⁴Institute of Radiochemistry and Radioecology, University of Pannonia, Egyetem str. 10, Veszprém, H-8200, Hungary, Phone: +36 88 624-789, Fax: +36 88 624-178, e-mail: kt@almos.uni-pannon.hu

⁵Szeged University, Department of Mineralogy, Geochemistry and Petrology 'Vulcano' Petrology and Geochemistry Research Group, 6722 Szeged, Egyetem str. 2, Hungary, e-mail: palm@geo.u-szeged.hu, *corresponding author

Abstract: The ²²⁰Rn and ²²²Rn concentration in the Úrkút Manganese Formation is anomalously high, and it causes health risk for the attendants of the Úrkút Manganese Mine. In this study we suggest a new model for the high ratio of different natural radionuclides by the new genetic model of the Úrkút Manganese Formation. Fossilized Fe-rich biomats were found in the whole section of the deposit. Based on these, the formation of different types of Mn-ores by one or two step microbial mediation can be assumed. The biomats represent large amounts of organic matter offering large surfaces with negative ligands, as well as poorly ordered mineral phases like ferrihydrite and clay minerals with large and reactive surfaces. These features offer high capability of cation binding, among them ions of radioactive elements, which could be fixed on the active or inactive organic matter, as well as on mineral surfaces. The decay of fixed nuclides could result high ²²⁰Rn and ²²²Rn concentration in the Úrkút Mine.

Keywords: biomats, black shale, geomicrobiology, radon, natural radionuclide

1. INTRODUCTION

1.1. Biomats

Biomats are the common appearance of local microbial communities, with diverse species and strains on different surfaces. The biomats are widespread from the guts of the animals to deep sea hydrothermal springs. In this paper, we discuss biomats as geobiological features, in the form of thin films and layers on the rock surfaces with variable thickness (from cm to m), which are built up by organic and inorganic matters. These biomats can selectively enrich ions, among them ions of radioactive elements. In a section the biomats show fine laminae, which differ in their colors, textures and

elemental contents (Fig. 1). The different laminae may indicate different species or strains with different metabolic activity, and some evolutionary change could be observable in the vertical (or sometimes horizontal) zonation as well. If the structure of the biomat is complex and there is available sunlight, the uppermost layer is enriched with cyanobacteria which are phototrophs, and the lowermost parts by methanotrophs as the chemical gradient decrease. Between these two layers, different chemotroph species live, and these species have complex ecological connection with each other from competition to cooperation (Krumbein et al., 2003; Konhasuer, 2007).

The appearance of the biomat could indicate the enrichment of some elements, usually they are

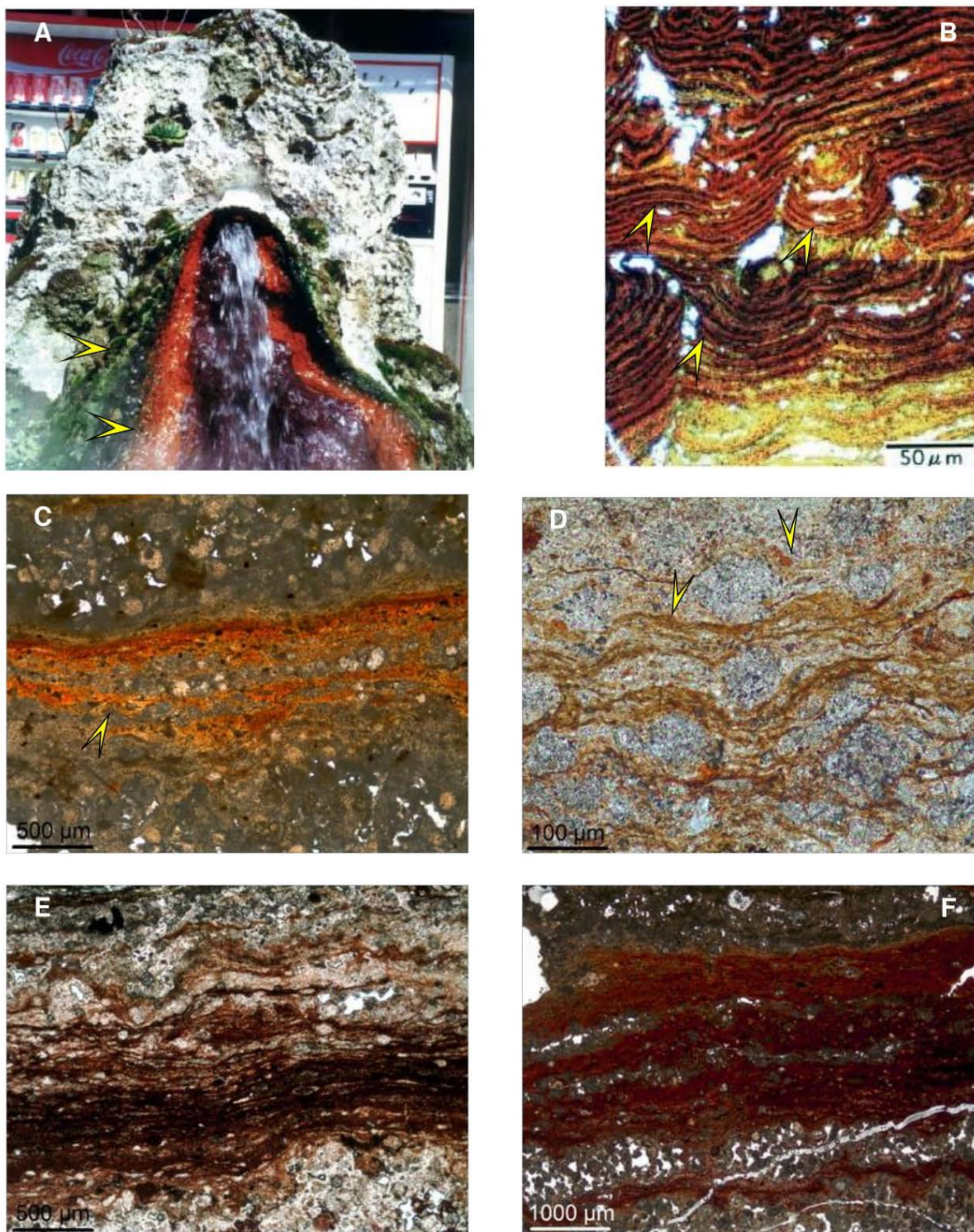


Figure 1. Biomats. (A) Recent biomat in a hot spring – the different color of the mat shows different metabolism (arrows, Hirayu, Japan); (B) Optical light micrograph of a fine laminated recent Fe-, Mn-rich biomat from Akayu hot spring (arrows, Iwo Jima, Japan) (Tazaki, 1999); (C-F) Fe-rich biomats (arrows) in quartz matrix in geysirite, Miocene age (15 My), Mátra Mts., Hungary (Photos by A. Müller)

formed on geochemical borders where the chemical gradient shows great change on a very small distance, like hot springs or estuarines.

The physical structure of the biomats is porous, web- or sponge-like, and water can stream through

freely. The chemical compounds of the biomats are the organic matter (lipids, steranes, enzymes, proteins, etc.) with mainly soluble inorganic content which are usually derived from cellular activity or from the bedrock (Konhauser, 2007).

By the metabolic activity of the microbes, different minerals could form from the soluble inorganic components. The elemental content of the minerals usually reflects the microbial metabolic preferences, but the first mineral phases which come out are usually poorly ordered with a high reactive surface (e.g. ferrihydrite, vernadite, clay minerals, etc.). These minerals could adsorb different atoms or ions, whether they are radiogenic or not, based on this feature, this mineral can act as a sorbent and retard migration in polluted environments.

Another process for cation retention is the high cation capacity of different types of the organic matter. Usually cell walls are encrusted by different molecules such as proteins or enzymes, which have multiple molecular structure and functional groups, but usually have some ligands with negative charge (e.g. $(OH)^-$ groups). These ligands could form binds with Ca^{2+} , Fe^{2+} , K^+ etc. cations, favoring mineral nucleation.

In special environments and results of the metabolic processes the biomats can be fossilized, in this occasion we can observe the fine laminae shown by different minerals and textures with the cyclicity of special organic matter (e.g. hopanes) (Wiener et al., 2003; Konhauser, 2007).

Ions of radioactive elements (e.g. Ra, U, Th, etc. and their decay daughter elements) can be enriched in biomats via an active or a passive way inside a very small area (a few m^2). As the isotopes decay, the area has anomalously high gamma ray, or radon content. Recently we have some reports about this phenomena (for details see Tsezos et al., 1987; Fujisawa & Tazaki, 2003; Tazaki, 2009; etc.), it usually appears in hot springs, where high natural radionuclide content of the water derived by the leaching of lower rocks. But we have less information about the formation and the pursuit of these kinds of biomats.

1.2. The Toarcian Úrkút Manganese Ore Deposit

The black shale-hosted Early-Jurassic (196 My) Úrkút Manganese Formation (ÚMF) is located at the central part of the Transdanubian Range (TR) (Fig. 2A) with a huge mass of economically important Mn ore (approx. 86 Mt metal content), which was embedded in Mesozoic limemarlstone (Fig. 2B). The ore deposit is built up by two main mineral phases (Mn oxide and carbonate minerals). The underground exploitation has occurred over a hundred years and ended in 2017 (Polgári et al., 2017).

The mineralogical and geochemical properties of the Mn ore deposit are characterized by Polgári et al.

(2012a) providing a new genetic model. They assume that the ore formed by a two-step microbial activity. Firstly, chemolithoautotrophic organisms oxidized the soluble metal cations (Mn^{2+} , Fe^{2+} etc.) into insoluble, poorly ordered mineral forms (manganite, vernadite, pyrolusite, cryptomelane, etc.) under oxic environmental conditions, where the source of the metal elements could have been a diffuse discharge hydrothermal activity (synsediment phase, sequestration of metals into the sediment as proto ore). Secondly, heterotrophic microbes could reduce the Mn- and Fe-oxide minerals to carbonate form (mainly rhodochrosite, as main ore mineral), via oxidizing the organic matter and mineralizing it in the form of carbonates during the early diagenetic processes under suboxic-anoxic environmental conditions (diagenetic phase).

Former studies show that the main primordial terrestrial isotopes (e.g. ^{238}U ; ^{232}Th ; ^{40}K) occur in manganese minerals in trace amounts (Grasselly & Pantó, 1988; Abel-Ghany, 2010). As Kávási et al. (2007, 2009) points out, in the caverns of the Úrkút Manganese Mine are high concentrations of Rn gas, the average ^{222}Rn values are $600 Bq/m^{-3}$ (without ventilation it reaches $2000-3000 Bq/m^{-3}$, and in caverns $10,000 Bq/m^{-3}$ also occurred). The average ^{220}Rn (thoron gas) values are $200-300 Bq/m^{-3}$ (without ventilation it reaches $1000 Bq/m^{-3}$). Vigh et al. (2013) discussed the enrichment of natural radionuclides and Rn in the different parts of the ore, while the K enriched in the green, celadonite-bearing Mn carbonate ore (average 2.29 wt. %), the U and Th enriched in the clay mineral rich black shale zones (1.9 and 8.4 ppm, respectively). It was shown that the geochemical behaviour of the parent and daughter isotopes is different. Comparing the rock types and the average activity concentrations of ^{232}Th , ^{234}Th and ^{226}Ra , there were ore horizons where parent favoured disequilibrium in U-series was detected, while at other horizons U has leached out leaving behind radium from which radon is produced (Vigh et al., 2013).

Previous interpretation summarized by Vigh et al. (2013) proposed the following aspects in the background of elevated radon concentration: (i) contribution of C_{org} in the formation of black shale and Mn-carbonate ore; (ii) P-rich layers represented by fish remnants in heterogenous distribution; (iii) clay-rich composition of the ore deposit (celadonite occurring in Mn carbonate ore, containing K), moreover, the adsorption characteristics of clay minerals should also be taken into account concerning the binding of natural radionuclides; (iv) the microbial mediation in formation processes of manganese mineralization, and the marine-geochemical relationship of U also preferred in microbial processes; (v) the effect of secondary

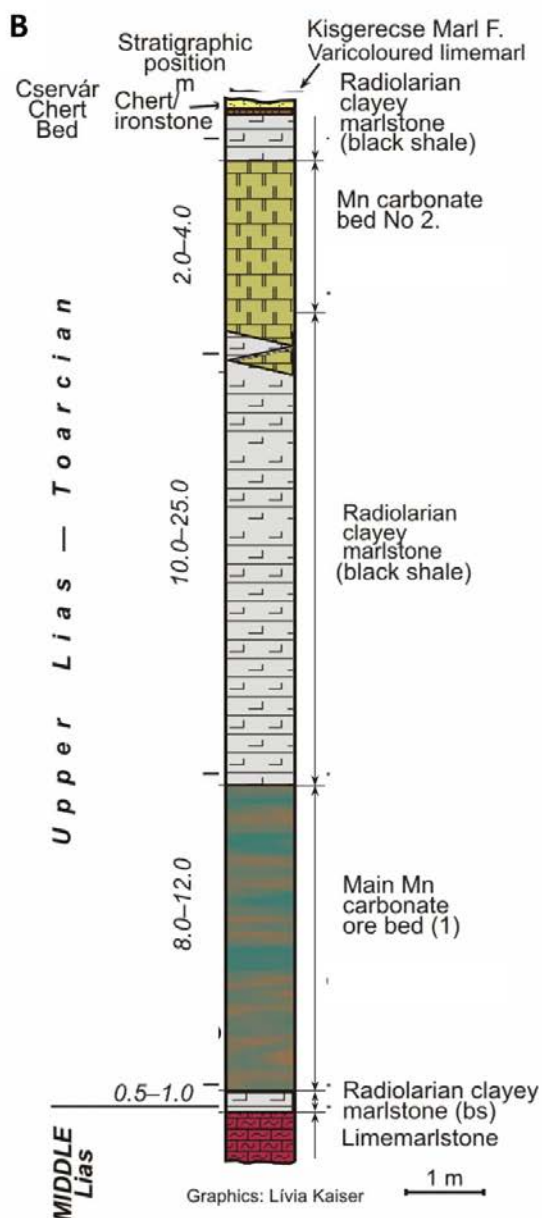
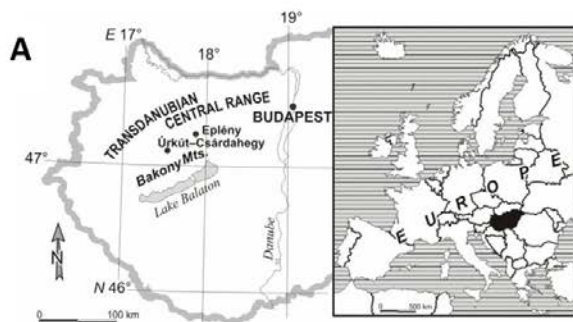


Figure 2. Locality of the Úrkút Manganese Formation (GPS coordinates: N 47°05'03.3"; E 17°38'30.6") (A) and the geological cross-section of the deposit (B)

oxidizing processes causing chemical transformations; (vi) in spite of the low U content of the deposit, high radon concentration occurs during

underground exploitation, as huge mass of the ore (ore types and black shale) is in contact with mine air representing the source of geo hazard.

As the contribution of biomat formation in the selective enrichment of natural radionuclides was not taken into consideration, so the aim of this paper is to provide evidences of this scenario, providing new data and also reviewing earlier considerations.

2. MATERIALS AND METHODS

The measurements were carried out on 54 samples collected from the different types of the initial (Mn oxide rich) part and the main carbonate ore bed of the deposit; 3 from the limemarlstone footwall, 6 from the oxide ore parts, 5 from the clay mineral-rich and 40 from the carbonate-rich ore zones (Table 1, Fig. 2B). Polished samples and thin sections were made for microtextural and micromineralogical studies.

An ECLIPSE 600 optical rock microscope was used (IGGR, HAS, Budapest, Hungary) for the microtextural and basic mineralogical examinations.

Based on these, the mineralogical and organic matter content was characterized by a Bruker VERTEX 70 Fourier transform infrared spectrometer (FTIR) equipped with a Bruker HYPERION 2000 microscope with a 20x ATR objective and MCT-A detector. During ATR analysis, the samples were contacted with a Ge crystal (0.5 micron) tip on the selected 1 N pressure. The measurement was conducted for 32 seconds in the 600–4000 cm^{-1} range with 4 cm^{-1} resolution. Opus 5.5 software was used to evaluate the data. For Mn oxide determination the equipment could not be used, as those peaks occur in the $<600 \text{ cm}^{-1}$ range.

All of the examinations were made on standard thin sections (7), and 21 spectra were acquired. During the FTIR investigations some types of organic matter (carbon-carbon bonds, carbon-hydrogen bonds, etc.) were characterized. Contamination of epoxy glue and glass were taken into consideration, and peaks of these phases were not considered.

Detailed high resolution petrological, mineralogical, geochemical (main and trace element, stable C, O, S isotope composition) and organic geochemical measurements and interpretation of a large sample set was also taken into consideration (Polgári et al., 2012ab, 2013, 2016ab).

3. RESULTS AND DISCUSSION

Based on the optical rock microscopy we assumed that the Mn oxide and carbonate ore have very heterogenous mineralogical content with typical textural elements. In the initial Mn ore as well as in the main Mn carbonate ore bed and the host black

Table 1. List of samples and used methods (Úrkút Mine, Shaft No. III, western minefield, deep level, +180 and +186 mBf)

No.	Samples	rock type	Ore zone	Methods							References
				A	B*	C*	D*	E*	F	G*	
1	2/4/A	footwall limemarlstone	footwall	X							Molnár et al., (2017)
2	2/4/B	footwall limemarlstone	footwall	X							↓
3	2/4/D	footwall limemarlstone	footwall	X							
4	1/1/A	initial Fe-Mn oxide	footwall	X	X		X		O		
5	1/1/B	initial Fe-Mn oxide	footwall	X	X		X		O		
6	1/1/C	initial Fe-Mn oxide	footwall	X	X		X	X	O		
7	1/1/D	initial Fe-Mn oxide	footwall	X	X		X	X	O	X	
8	2/1/A	initial Fe-Mn oxide	footwall	X	X		X	X	O		
9	2/1/B	initial Fe-Mn oxide	footwall	X	X		X	X	O		
10	2/2/A	clay mineral-rich footwall	footwall	X	X		X			X	
11	2/2/B	clay mineral-rich footwall	footwall	X	X		X			X	
12	2/3/A	clay mineral-rich footwall	footwall	X	X		X				
13	2/4/C	clay mineral-rich footwall	footwall	X	X			X	O		
14	2/4/E	clay mineral-rich footwall	footwall	X	X						
15	1/12	Radiolarian clayey marlstone	radiolarian clayey marlstone (Bs1)	X	X		X			X	Polgári et al. (2012a)
16	1/13	green type ore	main Mn carbonate ore bed	X	X		X			X	Polgári et al., (2012ab, 2013)
17	1/14	green type ore	main Mn carbonate ore bed	X	X		X			X	↓
18	1/15	green type ore	main Mn carbonate ore bed	X	X		X			X	
19	1/16	green type ore	main Mn carbonate ore bed	X	X		X			X	
20	1/17	green type ore	main Mn carbonate ore bed	X	X		X			X	
21	3/7	brown ore type	main Mn carbonate ore bed	X	X		X			X	
22	3/8	brown ore type	main Mn carbonate ore bed	X	X		X			X	
23	3/9	brown ore type	main Mn carbonate ore bed	X	X		X			X	
24	3/13	brown ore type	main Mn carbonate ore bed	X	X		X			X	
25	3/14	brown ore type	main Mn carbonate ore bed	X	X		X			X	
26	4/4	brown ore type	main Mn carbonate ore bed	X	X		X			X	
27	4/7	brown ore type	main Mn carbonate ore bed	X	X		X			X	

No.	Samples	rock type	Ore zone	Methods						References	
				X	X		X		X		
28	4/8	brown ore type	main Mn carbonate ore bed	X	X		X			X	
29	4/9	brown ore type	main Mn carbonate ore bed	X	X		X			X	
30	4/10	brown ore type	main Mn carbonate ore bed	X	X		X			X	
31	4/12	brown ore type	main Mn carbonate ore bed	X	X		X			X	
32	4/13	brown ore type	main Mn carbonate ore bed	X	X		X			X	
33	4/15	green type ore	main Mn carbonate ore bed	X	X		X			X	
34	4/16	green type ore	main Mn carbonate ore bed	X	X		X			X	
35	4/17	green type ore	main Mn carbonate ore bed	X	X		X			X	
36	4/19	green type ore	main Mn carbonate ore bed	X	X		X			X	
37	4/20	green type ore	main Mn carbonate ore bed	X	X		X			X	
38	4/23	green type ore	main Mn carbonate ore bed	X	X		X			X	
39	4/25	brown ore type	main Mn carbonate ore bed	X	X		X			X	
40	5/1	gray ore type	main Mn carbonate ore bed	X	X		X			X	
41	5/3	gray ore type	main Mn carbonate ore bed	X	X		X			X	
42	5/9	gray ore type	main Mn carbonate ore bed	X	X		X			X	
43	5/12	gray ore type	main Mn carbonate ore bed	X	X		X			X	
44	5/14	gray ore type	main Mn carbonate ore bed	X	X		X			X	
45	5/15	gray ore type	main Mn carbonate ore bed	X	X		X			X	
46	5/16	Radiolarian clayey marlstone	radiolarian clayey marlstone (Bs2)	X	X		X			X	Polgári et al. (2016ab)
47	5/17	Radiolarian clayey marlstone	radiolarian clayey marlstone (Bs2)	X	X		X			X	↓
48	5/18	Radiolarian clayey marlstone	radiolarian clayey marlstone (Bs2)	X	X		X			X	
49	5/19	Radiolarian clayey marlstone	radiolarian clayey marlstone (Bs2)	X	X		X			X	
50	Z/6	Mn carbonate	bed No. 2	X	X					X	Polgári et al., (2012a)
51	Z/7	Mn carbonate	bed No. 2	X	X					X	↓
52	Z/1	Radiolarian clayey marlstone	radiolarian clayey marlstone (Bs3-4)	X	X		X			X	Polgári et al., (2016ab)
53	Z/2	Radiolarian clayey marlstone	radiolarian clayey marlstone (Bs3-4)	X	X		X			X	↓
54	23/	Goethite and celadonite-bearing chert	overlying chert ironstone	X	X					X	Polgári et al. (2010)

Legend: *: investigation of samples are from references; Bs1- Radiolarian clayey marlstone below the main ore bed; Bs2- Radiolarian clayey marlstone between the main ore bed and bed No. 2; Bs3-4- Radiolarian clayey marlstone overlying bed No. 2. For details see Figure 2. ↓

A – rock microscopy; B – X-ray powder diffraction (XRD); C – Raman spectroscopy; D – Mass spectrometry (MS); E – Gas - chromatography mass spectroscopy (GC-MS); F - Fourier transform infrared spectroscopy (FTIR), O-recent study, sample number by italic letters; G – Chemical analysis (ICP, XRF, MP-AES)

List of minerals: rhodochrosite (MnCO_3); goethite (FeOOH); celadonite ($\text{K}(\text{Mg},\text{Fe}^{2+})\text{Fe}^{3+}(\text{Si}_4\text{O}_{10})(\text{OH})_2$); quartz (SiO_2)

The archive samples can be found at the storage of Institute for Geological and Geochemical Research, HAS.

shale, brownish, Fe-rich woven texture and filamentous forms were observed, as mineralized microbially produced sedimentary structures (MMPSS, Polgári et al., 2012ab; Fig. 3). With higher magnification, complex, pearl-necklace-like filamentous structures were observed, which resembled fossilized bacterial forms. Sometimes the Mn-rich parts had brighter bands, but it usually appeared on the contact zone of the ore and the footwall.

The clay mineral rich samples have heterogeneous mineral content, the Mn oxide-bearing parts occur with biodebris, and the greenish clay minerals usually appear in patches. In these samples, elongated brownish, Fe-rich lines and bands were characteristic (average thickness are 0.1-0.2 mm). It has the same tiny filamentous textural elements like the Mn oxide parts, but without oxidized Mn mineral forms and lower average quantity of Fe oxides. All of the ore parts have low biodebris content (mainly *Echinozoa* fragments). As a whole, the Mn deposit contains a series of Fe-rich biomats of micrometer scale, and at some places also macroscopic evidences of microbial contribution in the form of stromatolites can be seen (stromatolite is a geological structure from micrometer to some meters scale made by microbial contribution). Previous studies proved the Fe oxihydroxide (goethite-FeOOH) content of the filamentous forms as mineralized microbially produced sedimentary structures (MMPSS, Polgári et al., 2012b).

By the FTIR, the different Fe-oxide minerals such as goethite (wave number: 877 cm^{-1}), maghemite (wave number: 607 cm^{-1} and 697 cm^{-1}) and ferrihydrite (wave number: 602 cm^{-1}) were characterized (Table 2). Beside these, clay minerals (wave number 990 cm^{-1}) were also identified, but this method cannot be useful for the identification of different Mn oxides and the prompt characterization of clay minerals, so former studies were also taken into consideration (e.g. Polgári et al., 2012ab; 2013, 2016ab), which found manganite, pyrolusite, vernadite, Ba- and K-rich Mn minerals. The organic matter content shows selective enrichment with the band-like Fe-rich zones, but the quantitative measurements were not possible because of the superposition of the peaks which belong to the organic and inorganic matter. The organic matter content of the Fe-rich zones is diverse, C-C (wave number: 1602 cm^{-1}), C-O (wave number: 1155 cm^{-1}) and C-H single and double bonds (wave number: 2852 cm^{-1} and 2926 cm^{-1}) were identified. At two areas aromatic groups (wave

number: 3090 cm^{-1}) were also detected.

Based on these results it can be assumed that series of fossilized biomats were identified, all of the micro- and macrotectural features support this scenario (filamentous, pearl-necklace-like forms and banded-like occurrences of different mineral phases, stromatolite-like appearance) with the mineralogical (different Fe- and Mn-minerals, with high ratio of poorly ordered phases) and geochemical (selective enrichment of the different types of organic matter with the Fe-, Mn-rich mineral phases) data support this. Concerning recent results, which focused to the initial phase of the manganese mineralization, series of similar Fe-bioma-like forms were detected which are common in the different types of the main Mn carbonate ore bed (Polgári et al., 2012ab).

As Vigh et al. (2013) showed, the U and Th concentration was enriched in the black shale parts of the ore deposit, so we assume that in that part of the ore the biological effects were weaker than the geochemical properties (e.g. reductive environment is needed to the immobilization of the U cations). While in the initial oxide ore, there was indication that K was enriched in the clay minerals, causing higher radiation via the decay of the ^{40}K isotope, the Rn could appear in the oxide parts too, by the former cellular activity, which enriched the Ra content by the material of the bacterial metabolism (e.g. like co-fluctuation). The determination of distribution of Ra content in the profile needs further investigation.

As the natural radionuclides content of the footwall limemarlstone is low, and on the other hand the initial part of Mn mineralization also contains series of biomats (Molnár, 2015; Molnár et al., 2017 and recent study), the role of high reactive surface of the poorly crystallized Fe- Mn oxides and the absorption capacity of clay minerals also could be important.

4. CONCLUSION

In this study it was shown that former biological activity could form diverse mineral association with extensive areal occurrence and microbial activity could result ores with great economic importance. The biologically (microbially) mediated ore formation is a complex process, the role of microbes needs complex investigation from macro to micro scales, including the inorganic and organic compounds.

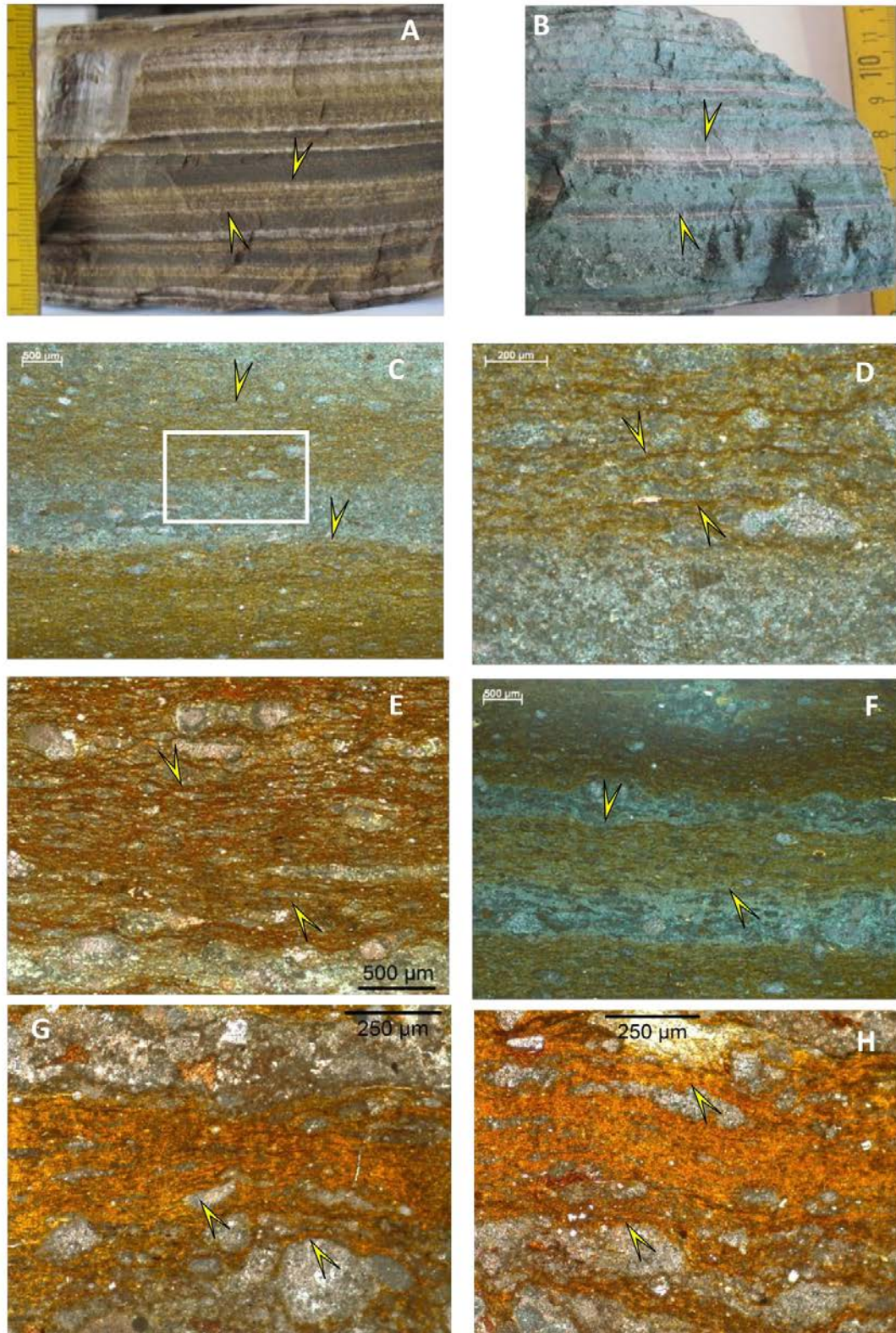


Figure 3. Representative fine-laminated Mn carbonate ore samples (cut surfaces) (A-B) and microtexture. (A) Brown Mn carbonate ore, sample No. 3/8; (B) Green Mn carbonate ore, sample No. 1/13; (C-H) Series of Fe-rich biomats in the main Mn carbonate ore, representative images (arrows). (C) Sample No. 4/19; (D) Enlarged part of signed area (C); (E) Sample No. 4/20; (F) Sample No. 4/23; (G-H) Sample No. 4/7. (The matrix is Ca-rhodochrosite, celadonite and smectite, Jurassic age (196 My), Úrkút, Bakony Mts., Hungary. (C-H) optical rock microscopy, transmitted light, 1 Nicol; Photos by A. Müller and M. Polgári)

Table 2. Mineral phase and organic material composition and frequency of phases in FTIR spectra

Mineral phase	References	Wavelength [cm ⁻¹]	Sample ID*						
			1/1/A	1/1/B	1/1/C	1/1/D	2/1/A	2/1/B	2/4/C
		Total No. of spectra→	1	3	5	2	2	4	4
ferrihydrite	Glotch & Rossman 2009	604	0	0	2/5	2/2	1/2	2/4	2/4
maghemite	Glotch & Rossman 2009	607, 637	0	1/3	2/5	0	0	1/4	1/4
akaganeite	Glotch & Rossman 2009	663, 787	0	1/3	4/5	2/2	0	1/4	0
rhodochrosite	Müller et al., 2014	712, 864,	1/1	3/3	2/5	0	1/2	2/4	2/4
Si-O stretching of quartz	Madejová & Komádel, 2001	776	0	0	0	0	1/2	0	2/4
goethite	Glotch & Rossman 2009	877	0	1/3	3/5	2/2	0	0	0
chlorite	Udvardi et al., 2014	980	0	1/3	3/5		1/2	1/4	1/4
clay (kaolinite/montmorillonite)	Madejová & Komádel, 2001; Madejová, 2003	989, 1000, 3570	0	1/3	3/5	2/2	2/2	1/4	0
apatite	Figuerido et al., 2012; Beasley et al., 2014; Veiderma et al., 1998	793, 1012-1031	0	0	2/5	0	0	1/4	2/4
Organic compounds									
v s C-O-C, C-C	Parikh & Chorover, 2006	1078	0	0	1/5	0	0	1/4	1/4
v C-O	Parikh & Chorover, 2006	1170	0	0	0	0	1/2	1/4	1/4
vs CO	Parikh & Chorover, 2006	1360-1450	0	0	0	0	0	1/4	0
d CH ₂	Parikh & Chorover, 2006	1454-1482	0	0	2/5	2/2	0	3/4	2/4
C-N, CH deformation in PAHs	Parikh & Chorover, 2006	1526	0	0	1/5	1/2	0	0	0
C-N N-H amide II in PAHs	Parikh & Chorover, 2006	1540-1550	0	0	1/5	0	0	3/4	0
C=C asym. stretch	Parikh & Chorover, 2006	1598	1/1	0	0	0	1/2	3/4	1/4
amide I C=O, C-N, N_H in PAHs	Parikh & Chorover, 2006	1632-1652	0	1/3	4/5	2/2	0	0	1/4
v as COOH	Parikh & Chorover, 2006	1720-29	1/1	0	1/5	2/2	0	1/4	0
C=O	Parikh & Chorover, 2006	1799	0	1/3	1/5	1/2	0	0	0
C=O	Müller et al., 2014	2343	1/1	0	0	0	0	0	0
C=O	Müller et al., 2014	2365	1/1	0	0	0	0	0	0
C-H sym. stretch CH ₂ (long chain CH)	Parikh & Chorover, 2006	2853	1/1	1/3	4/5	2/2	1/2	3/4	2/4
C-H asym. Stretch CH ₂ (long chain CH)	Parikh & Chorover, 2006	2926	1/1	1/3	4/5	2/2	1/2	3/4	2/4
combination band of NH ₄	Madejová & Komádel, 2001	3047	0	0	0	2/2	0	0	2/4
C-H stretch aromatic ring (long chain CH)	Parikh & Chorover, 2006	3090	0	1/3	3/5	0	0	0	0

*For details see Table 1.

The new genetic model of the Úrkút Manganese Ore Deposit supports this purpose, offering a frame for the case study of high refinement investigations. The microbially mediated mineralization provided an ideal situation for the cation sequestration (high reactive surface of the poorly ordered mineral phases), among them ions of radioactive elements together with the organic matter. Some metabolic activity could induce the enrichment of some chemical compounds with high radioactive radiation (e.g. the bacterial co-fluctuation of Ra isotopes). Macro- and microtextural features and the mineral composition supports this scenario. In the case

of high cation capacity, and the large amount of ore material produced by microbially mediated mineralization, the mineral procession and mining activity must be made with caution, because of the possibility of health risk of the potentially high ratio of radioactivity.

ACKNOWLEDGEMENTS

The authors thank the support of National Research, Development and Innovation Office, National Scientific Research Found No. 125060. We appreciate the

constructive contribution of Zsombor Molnár, technical assistance and photos of Alexandra Müller (IGGR, RCAES HAS, Budapest, Hungary). We thank the careful reviews and constructive suggestions provided by the anonymous reviewers, and editorial handling.

REFERENCES

- Abel-Ghany, H.A., 2010. *Natural activities of 238-U, 232-Th, 40-K in Manganese Ore*. American Journal of Environmental Sciences, 6, 88–92.
- Beasley, M.M., Bartelink, Eric J., Taylor, L. & Miller, R., 2014. *Comparison of transmission FTIR, ATR, and DRIFT spectra: implications of assesment of bone bioapatite diagenesis*. Journal of Archeological Science, 46, 16–22.
- Figueiredo, M.M., Martins, A.G. & Gamelas, J.A.F., 2012. *Characterization of bone and bone-based graft materials using FTIR spectroscopy*. INTECH Open Access Publisher.
- Fujisawa, A. & Tazaki, K., 2003. *The radioactive microbial mats – In case of Misasa hot springs in Tottori Prefecture*. In: Katama N. (ed.): Proceedings: International Symposium of the Kanazawa University 21st-Century COE Program Vol. 1., Kanazawa University, Kanazawa, Japan, 328–331.
- Glotch, T.D. & Rossman, G.R., 2009. *Mid-infrared reflectance spectra and optical constants of six iron oxide/oxyhydroxide phases*. Icarus, 204, 663–671.
- Grasselly, Gy. & Pantó, Gy., 1988. *Rare Earth Elements in the Manganese Ore deposit of Úrkút (Bakony Mountains, Hungary)*. Ore Geology Reviews, 4, 115–24.
- Kávási, N., Németh, Cs., Kovács, T., Tokonami, S., Jobbágy, V., Várhegyi, A., Gorjánác, Z., Vigh, T. & Somlai, J., 2007. *Radon and thoron parallel measurements in Hungary*. Radiation Protection Dosimetry, 123, 250–3.
- Kávási, N., Somlai, J., Vigh, T., Tokonami S., Ishikawa, T., Sorimachi, A. & Kovács, T., 2009. *Difficulties in the dose estimate of workers originated from radon and radon progeny in a manganese-mine*. Radiation Measurements, 44, 300–5.
- Konhauser, K.O., 2007. *Intoduction to geomicrobiology*, Blackwell publish, 43–67.
- Krumbein, W.E., Ulrike, B., Gorbushina, A.A., Levit, G. & Palinska, K.A., 2003. *Biofilm, Biodictyon and Biomat - Biolaminites, Oolites, Stromatolites* – In: Geophysiology, Global Mechanism and Parahistology, in Fossil and Recent Biofilms (edited by Krumbein W. E., Patterson, D., Zavarzin, G. A.), Springer Science Media, Dordrecht, 1–29.
- Madejová, J. & Komadel, P., 2001. *Baseline studies of the clay minerals society source clays: infrared methods*. Clays and Clay Minerals, 49, 410–432.
- Madejová, J., 2003. *FTIR techniques in clay mineral studies*. Vibrational spectroscopy, 31/1, 1–10.
- Molnár, Zs., 2015. *Initial Fe-Mn-oxide ore indications in the footwall of the Toarcian Úrkút Mn-carbonate ore deposit, Hungary*. Thesis. Eötvös University, Budapest, 208 p.
- Molnár, Zs., Polgári, M., Hein, J.R., Józsa, S., Fekete, J., Gyollai, I., Fintor, K., Bíró, L., Szabó, M., Rapi, S., Forgó, P. & Vigh T., 2017. *Fe-Mn oxide indications in the feeder and mound zone of the Jurassic Mn-carbonate ore deposit, Úrkút, Hungary*. Ore Geology Reviews, 86, 839–855.
- Müller, C.M., Pejčić, B., Esteban, L., Delle Piane, C., Raven, M. & Mizaikoff, B., 2014. *Infrared Attenuated Total Reflectance Spectroscopy: An Innovative Strategy for Analyzing Mineral Components in Energy Relevant Systems*. Scientific Reports 4.
- Parikh, S.J. & Chorover, J., 2006. *ATR-FTIR spectroscopy reveals bond formation during bacterial adhesion to iron oxide*. Langmuir, 22/20, 8492–8500.
- Polgári, M., Hein, J.R., Bíró, L., Gyollai, I., Németh, T., Sajgó, Cs., Fekete, J., Schwark, L., Pál-Molnár, E., Hámor-Vidó, M. & Vigh, T., 2016a. *Mineral and chemostratigraphy of a Toarcian black shale hosting Mn-carbonate microbialites (Úrkút, Hungary)*. Palaeogeography, Palaeoclimatology, Palaeoecology, 459, 99–120.
- Polgári, M., Hein, J.R., Fórizs, I., Vigh, T., Szabó-Drubina, M., Bíró, L., Müller, A. & Tóth, A.L., 2012a. *Microbial processes and the origin of the Úrkút manganese deposit, Hungary*. Ore Geology Reviews, Special Issue “Manganese Metallogenesis” 47, 87–109.
- Polgári, M., Hein, J.R., Németh, T., Pál-Molnár, E. & Vigh, T., 2013. *Celadonite and smectite formation in the Úrkút Mn-carbonate ore deposit (Hungary)*. Sedimentary Geology, 294, 157–163.
- Polgári, M., Hein, J.R., Tóth, A.L., Pál-Molnár, E., Vigh, T., Bíró, L. & Fintor, K., 2012b. *Microbial action formed Jurassic Mn-carbonate ore deposit in only a few hundred years (Úrkút, Hungary)*. Geology, 40(10), 903–906.
- Polgári, M., Hein, J.R., Tóth, M., Brukner-Wein, A., Vigh, T., Bíró, L. & Cserhádi, C., 2010. *Lias manganese deposits, Hungary Genesis of a regionally widespread celadonitic chert ironstone bed overlying Upper Lias manganese deposits, Hungary*. Journal of the Geological Society London, 167, 313–328.
- Polgári, M., Németh, T., Pál-Molnár, E., Futó, I., Vigh, T. & Mojzsis, J.S., 2016b. *Correlated chemostratigraphy of Mn-carbonate microbialites (Úrkút, Hungary)*. Gondwana Research, 29, 1, 278–289.
- Polgári, M., Szabó, Z. & Vigh, T., 2017. *Manganese ore mining at Úrkút (1917-2017)*, GeoLitera Publishing House, Szeged, 260p. (ISBN 978-963-306-547-1).
- RUFF Database**
- Tazaki, K., 1999. *Architecture of biomats reveals history of geo-, aqua-, and bio-systems*. Episodes, 22(1), 22–23.
- Tazaki, K., 2009. *Observation of microbial mats in radioactive hot springs*. Science Reports of Kanazawa University 53, 25–37.
- Tsezos, M., Baird, I.H. & Shelmit L.W., 1987. *Elution of*

- Radium adsorbed by microbial mats.* Chemical Engineering Journal, 34, B57-B64
- Udvardi, B., Kovács, I. J., Kónya, P., Földvári, M., Fűri, J., Budai, F., Falus, Gy., Fancsik T., Szabó Cs., Szalai Z. & Mihály, J.,** 2014. *Application of attenuated total reflectance Fourier transform infrared spectroscopy in the mineralogical study of a landslide area, Hungary.* Sedimentary Geology, 313, 1–14.
- Veiderma, M.I.H.K.E.L., Knubovets, R.E.N.A. & Tonsuaadu, K.,** 1998. *Structural properties of apatites from Finland studied by FTIR spectroscopy.* Bulletin Geological Society of Finland, 70, 69–75.
- Vigh, T., Kovács, T., Somolai, J., Kávási, N., Polgári, M. & Bíró, L.,** 2013. *Terrestrial radioisotopes in black shale hosted Mn-carbonate deposit (Úrkút, Hungary).* Acta Geophysica, 61(4), 831–847
- Wiener, S., Dove, P.M. & De Yoreo, J.J.,** 2003. **Biom mineralization,** Reviews of Mineralogy and Geochemistry, 54, 15–113.

Received at: 30. 01. 2018

Revised at: 19. 02. 2018

Accepted for publication at: 18. 03. 2018

Published online at: 22. 03. 2018